Sub-100-nm negative bend resistance ballistic sensors for high spatial resolution magnetic field detection

A. M. Gilbertson, D. Benstock, M. Fearn, A. Kormányos, S. Ladak, M. T. Emeny, C. J. Lambert, T. Ashley, S. A. Solin, and L. F. Cohen
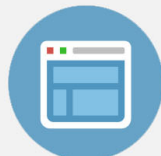
Sub-100-nm negative bend resistance ballistic sensors for high spatial resolution magnetic field detection

A. M. Gilbertson,[1,a)] D. Benstock,[1] M. Fearn,[2] A. Kormányos,[3] S. Ladak,[1] M. T. Emeny,[2] C. J. Lambert,[3] T. Ashley,[2] S. A. Solin,[1,4] and L. F. Cohen[1]

[1]*Blackett Laboratory, Imperial College London, Prince Consort Rd., London SW7 2BZ, United Kingdom*
[2]*QinetiQ, St. Andrews Road, Malvern, Worcestershire WR14 3PS, United Kingdom*
[3]*Department of Physics, Lancaster University, Lancaster LA1 4YB, United Kingdom*
[4]*Department of Physics and Center for Materials Innovations, Washington University in St. Louis, St. Louis, Missouri 63130, USA*

We report the magnetic field detection properties of ballistic sensors utilizing the negative bend resistance of $InSb/In_{1-x}Al_xSb$ quantum well cross junctions as a function of temperature and geometric size. We demonstrate that the maximum responsivity to magnetic field and its linearity *increase* as the critical device dimension is reduced. This observation deviates from the predictions of the classical billiard ball model unless significant diffuse boundary scattering is included. The smallest device studied has an active sensor area of 35×35 nm^2, with a maximum responsivity of 20 kΩ/T, and a noise-equivalent field of 0.87 μT/$\sqrt{Hz}$ at 100 K. © *2011 American Institute of Physics*. [doi:10.1063/1.3554427]

There is an ongoing drive to develop noninvasive magnetic field sensors with ultrahigh spatial resolution (UHSR) on the order of 100 nm or less for biomedical[1] and security applications. Conventional solid state sensors [e.g., Hall effect[2] or extraordinary magnetoresistance (EMR)[3]] rely on diffusive transport where materials with high carrier mobility (μ) are favorable for high magnetic field resolution. For this reason, experiments have largely focused on III-V semiconductors, although graphene[4] is clearly a future contender. At dimensions less than the electron mean free path ($\lambda_0 = \hbar k_F \mu / e$, where k_F is the Fermi wave vector), electrical transport becomes ballistic. A detailed understanding of how ballistic effects impact the detection properties is essential to optimize the performance of UHSR III-V sensors.

Here we show that the negative bend resistance (NBR) response $R_B(B)$ of a ballistic cross junction offers new opportunities for realizing UHSR if significant diffuse boundary scattering can be created in the device leads. The significance of this effect in terms of device scaling and detection properties that we report has not previously been appreciated. Under these conditions the maximum magnetic responsivity (R'_{max}) and its linearity increase as the critical dimensions of the device are reduced. We also show that R'_{max} can be substantially greater than the equivalent Hall coefficient and exhibits a large tunability with respect to geometric design. Our experimental observations are supported by classical billiard ball simulations.

The ballistic Hall response is sensitive to the average magnetic flux[5] within the sensor area (A) but is highly nonlinear and even suppressed at low fields. In contrast, the NBR observed in the same cross geometry was sensitive to the average flux and also to the spatial distribution of flux within A and was found to be favorable for the detection of small magnetic fields.[5,6] We have studied the size and temperature dependence of the NBR detection properties of InSb/InAlSb submicron crosses with critical dimensions

(lead width) down to 35 nm. For geometrically equivalent crosses (e.g., square), the classical model[7] for ideal hard wall specular boundaries predicts that R'_{max} is independent of the lead width due to a universal scaling of the $R_B(B)$ curves. Our results show a very different behavior which we explain by considering the influence of partially diffuse boundary scattering.

The sample used is a modulation doped $InSb/In_{1-x}Al_xSb$ heterostructure with a 30 nm InSb quantum well (QW) buried 50 nm beneath the surface.[8] The electron density (n_{2D}) and mobility of the as-grown wafer at 2 K were $n_{2D}=3.95 \times 10^{15}$ m^{-2} and $\mu=19.5$ m^2/V s, corresponding to $\lambda_0 = 2.03$ μm and a Fermi wavelength $\lambda_F = 40$ nm. Cross structures were defined using e-beam lithography and a shallow (≈ 135 nm) reactive ion etch in a CH_4/H_2 plasma, providing hard wall confinement [Figs. 1(a) and 1(b)]. A rough etched
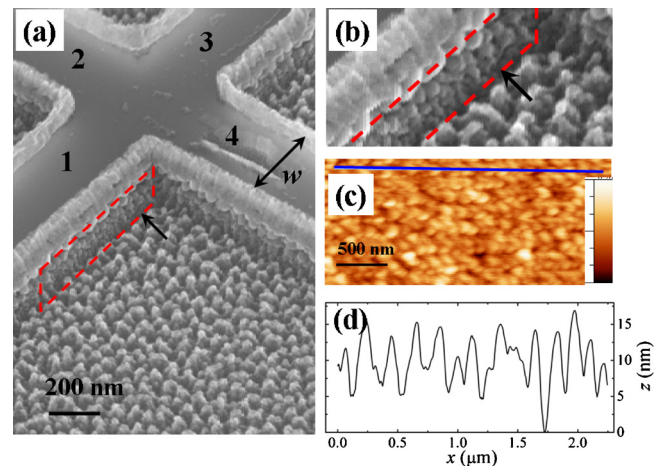

FIG. 1. (Color online) (a) Scanning electron microscopy micrograph of a $w=400$ nm cross and lead configuration. Residual polymer/resist is present on the mesa edge. The dashed area indicates the mesa sidewall, shown close up with a 2× magnification in (b). (c) AFM scan of etched surface with rms $\Delta=3.8$ nm. The z-scale is 32 nm. (d) A line scan taken across the AFM as indicated in (c), illustrating the typical surface profile.

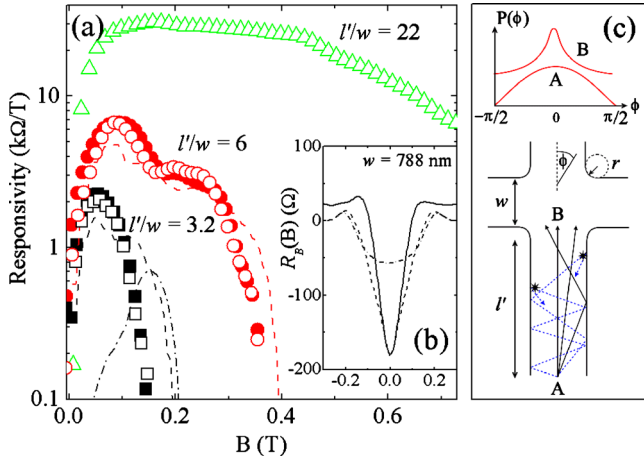a)Electronic mail: adam-maurick.gilbertson@imperial.ac.uk.

FIG. 2. (Color online) (a) Low temperature responsivity $R'(B)$ for devices of varying width at 40 K (open symbols) and 10 K (closed symbols); $w_{eff} = 788$ (□), 264 (○), and 35 nm (△). Simulations (0 K) of $R'(B)$ for $p = 0.8$ are indicated by the dashed lines for comparison to the 10 K data. The dotted line shows a simulation for the 788 nm device with $p = 1$. Inset: comparison of the NBR response $R_B(B)$ of the 788 nm device at 10 K (solid line) to simulations with $p = 1$ (dotted line) and $p = 0.8$ (dashed line) ($k_F = 1.56 \times 10^8$ m^{-1}, $r = 100$ nm). (c) Schematic diagram of a device lead illustrating diffuse collimation.

surface morphology is obtained, typical for CH_4/H_2 etching of In containing compounds.[9] Figure 1(c) shows an atomic force microscopy (AFM) scan of the etched surface; a rms roughness of $\triangle = 3.8$ nm (over 2.5×2.5 μm^2) is low, although not typical of InSb etching.[9] Figure 1(d) shows a line scan across the AFM image to illustrate the lateral profile of the roughness; Fourier analysis reveals two dominant frequencies corresponding to 160 and 215 nm. The latter can be considered as a lower limit for the correlation length (Λ) of the roughness. The device geometry is characterized by leads of physical width w and length l', with a radius of curvature at the junction corners (r) that is nominally zero, although some rounding ($r \approx 100$ nm) is inevitable in the fabrication process [cf. Fig. 2(c)]. Results are presented from devices with $w = 924$, 400, and 171 ± 15 nm and $l' = 2.5$, 1.6, and 0.8 ± 0.05 μm, respectively. The sidewall depletion width (w_{dep}) was deduced from magnetodepopulation measurements in quantum wires to be ≈ 68 nm, resulting in effective electrical widths ($w_{eff} \approx w - 2w_{dep}$) for our device leads of 788, 264, and 35 nm, respectively.[8] The two-terminal resistances (R_{2t}) of the devices in order of decreasing size are 10, 24, and 55 kΩ, respectively. These rather large values are due to the narrow leads. Four-terminal NBR measurements $R_B = (V_4 - V_3)/I_{1,2}$ [see Fig. 1(a)] were performed in the temperature range $2 \le T \le 300$ K using a lock-in technique with magnetic field applied perpendicular to the plane of the QW. The 35 nm device was depleted below 30 K, so in this case data are presented for $T \ge 40$ K.

To understand the influence of diffuse boundary scattering on the device properties, we have performed classical simulations of the NBR using the model of Beenakker and van Houten[7] that treats ballistic electrons as classical particles that are injected at the Fermi velocity and rebound from the sidewalls until they exit via one of the leads. Partially diffuse boundary scattering is introduced according to the approach of Blaikie *et al.*, via a single specularity parameter $0 \le p \le 1$, such that $p = 1$ corresponds to pure specular scattering.[10] Note that p is a property of the boundaries: it is

not expected to vary significantly between devices fabricated under the same conditions. The input parameters are w, l', r, $k_F = (2\pi n_{2D})^{1/2}$, and p.

The low temperature (10 K) NBR response from the 788 nm device is shown by the solid line in Fig. 2(b). The features are typical of all devices studied although both the amplitude and full width at half maximum of the NBR increase as the lead width w_{eff} is reduced (not shown). We compare the responsivity $R'(B) = \partial R_B / \partial B$ of all the devices at 40 K (open symbols) in Fig. 2(a). A marked dependence on w_{eff} is found; as w_{eff} is decreased from 788 to 35 nm, (i) a dramatic increase in the maximum responsivity (R'_{max}) is observed, reaching a value of 30 kΩ/T in the latter, and (ii) the field range over which this large R' is obtained increases, indicating an increased linearity of the NBR response.

The dotted-dashed line in Fig. 2(b) shows the simulation (0 K) of $R_B(B)$ for the 788 nm device using experimental parameters and assuming specular scattering ($p = 1$). The enhancement of the experimental NBR amplitude by a factor of 3 over the $p = 1$ simulation can be attributed to the existence of diffuse scattering (i.e., $p < 1$).[10] Further, a probability of diffuse scattering $(1-p) \approx 0.2-0.3$ can be deduced from our experimental results (10 K) by direct comparison to simulations. The dashed line in Fig. 2(b) shows the best fit to the experimental $R_B(0)$ obtained with $p = 0.8$ (a more detailed analysis is given in Ref. 8). The origin of the enhanced NBR is the *diffuse collimation* of ballistic electrons emitted into the device active area, as illustrated schematically in Fig. 2(c); electrons that are injected into the lead (point A) with an angular distribution of $P(\phi) = \cos(\phi)/2$ (ϕ is the angle with respect to the lead axis)[7] exit the lead (point B) with a distribution more strongly peaked in the forward direction due to an increased backscattering of electrons with large angle trajectories. This has the consequence of reducing the transmission into the side leads which enhances the NBR. Crucially, this collimation is sensitive not only to p but also to the ratio l'/w since this directly affects the interaction with the boundaries.

Interestingly, we find that universal scaling of R_B (and independence of R'_{max} on w_{eff}) is maintained for $p < 1$ when l'/w, r/w, and p are fixed. In our devices l'/w varies from 3.2 to 22 as the device dimensions are reduced and one expects a significant change in collimation and $R'(B)$. The dashed lines in Fig. 2(a) show the simulated $R'(B)$ curves for the 788 and 264 nm devices using $p = 0.8$ and experimentally determined values of w, k_F, and l' (the classical model is no longer valid in the smallest device where the number of transverse modes is $\sim 1-2$). Excellent agreement is found for both the larger devices with no fitting parameters, demonstrating that R'_{max} can be tuned via the geometrical parameter l'/w. The lower inset to Fig. 3 shows the predicted relationship between R'_{max} and l'/w ($p = 0.8$) and our experimental exploration of the parameter space from our devices at 40 K. Reasonable agreement is found. In principle, $l' \le \lambda_0$, therefore the maximum enhancement in $R'(B)$ is obtained in devices with narrow leads (where $\lambda_0/w \gg 1$). Furthermore, the increased range in B over which this large R' is obtained in this regime [Fig. 2(a)] is attractive for detection.

Finally, for a perfectly symmetric cross, $R'(B=0) = 0$. For the 35 nm device, $R'(B=0) = -4.1$ kΩ/T at 40 K, indicating a small geometric asymmetry in the placement or width of the leads. The exploitation of this asymmetry would
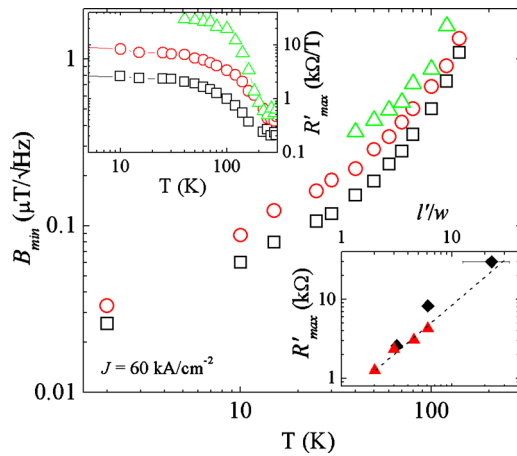
FIG. 3. (Color online) Temperature dependence of the noise-equivalent field B_{min} for devices in the thermal noise; w_{eff}=788 ($\square$), 264 ($\bigcirc$), and 35 nm ($\triangle$). Top inset: temperature dependence of R'_{max} for the devices. Bottom inset: dependence of R'_{max} on l'/w for the devices at 40 K ($\blacklozenge$) compared to simulations with p=0.8 ($\blacktriangle$). The dashed line is a guide for the eyes.

provide an obvious route to shift the location of R'_{max} toward B=0, thus "self-biasing" the device and enabling detection of ultrasmall magnetic fields.

A pronounced decay in R'_{max} is observed above 100 K in each device as shown in Fig. 3 (inset). This coincides with the decay in the NBR anomaly (not shown). The amplitude of the NBR is proportional to the fraction of electrons that travel ballistically across the device estimated by $\exp[-w_{eff}/\lambda_0(T)]$ and can be directly correlated with the responsivity.[11] As temperature is increased, the NBR will decay as phonon scattering processes reduce λ_0. However, the observed decay in R'_{max} is much greater than that expected from the change in λ_0 alone. The extreme case is the 35 nm device, which at 140 (40) K [where $\lambda_0 \approx 1.1$ (2.0) μm in the bulk] we estimate that $\approx$97% (98%) of electrons are ballistic, in which case both $R_B(B)$ and R' should retain much of their low temperature character. We propose that the decay of R'_{max} above 100 K originates from a different effect. This is attributed to the onset of intrinsic conduction in the volume of surrounding (shallow etched) $In_{1-x}Al_xSb$ buffer layer that provides a parallel conduction path,[12,13] leading to spurious transport that currently limits the device operation.

If we compare the low temperature R'_{max} figures to the conventional Hall responsivity of the devices, i.e., the Hall coefficient, R_H=$1/n_{2D}e$=1.4–2.8 kΩ/T, obtained at higher fields where classical behavior is recovered, we see that as the device dimensions are reduced R'_{max} exceeds R_H by a factor 10.

For comparison with field sensors of similar dimensions, the reported values of R'_{max} at 300 K for InAs (Ref. 14) and InSb (Ref. 3) EMR sensors with A=50$\times$150 nm^2 and 30$\times$35 nm^2 are 67 and 147 Ω/T, respectively, at a bias field of $\approx$100 mT. At 100 K (the highest temperature at which we can neglect parallel conduction), a 35 nm NBR sensor exhibits an R'_{max} over 100 times greater than these figures in a bias field of 200 mT. This demonstrates the clear potential of ballistic NBR devices.

The minimum detectable field or noise-equivalent field in the Johnson noise limit is B_{min}=$\sqrt{4k_BTR_{2t}\Delta f}/I_{max}R'_{max}$, where I_{max} is the maximum bias current, k_B is the Boltzmann constant, and Δf is the measurement bandwidth. In Fig. 3 we show the temperature dependence of B_{min} calculated for Δf=1 and a current density J=60 kA/cm^2 (the largest J explored). At 2 (100) K, sensitivities as small at 25 (500) and 33(680) nT/$\sqrt{Hz}$ are obtained in the 788 and 264 nm sensors. The 35 nm sensor has a $B_{min} \approx 0.36$ (0.87) μT/$\sqrt{Hz}$ at 40 (100) K. Optimization of the lead resistance and geometry will further improve the performance.

Previous reports on mesoscopic narrow gap InSb and InAs devices have only described specular boundary scattering.[15,16] We propose that partially diffuse boundary scattering is taking place within the leads of our devices due to the sidewall roughness indicated in Fig. 1(b), produced by the particular hard wall confinement technique. Assuming that the surface roughness is directly translated onto the sidewalls during the etch process, this would result in $\Lambda/\lambda_F \approx 5$.[17]

In summary, the enhanced and tunable responsivity of InSb NBR sensors that results from partially diffuse boundary scattering is extremely promising for UHSR detection particularly if the parallel conduction problem can be resolved.

[1]P. Manandhar, Nanotechnology **20**, 355501 (2009).
[2]A. Sandhu, Microelectron. Eng. **73–74**, 524 (2004).
[3]S. A. Solin, D. R. Hines, A. C. H. Rowe, J. S. Tsai, Y. A. Pashkin, S. J. Chung, N. Goel, and M. B. Santos, Appl. Phys. Lett. **80**, 4012 (2002).
[4]S. Pisana, P. M. Braganca, E. E. Marinero, and B. A. Gurney, Nano Lett. **10**, 341 (2010).
[5]F. M. Peeters and X. Q. Li, Appl. Phys. Lett. **72**, 572 (1998).
[6]M. Hara, J. Shibata, T. Kimura, and Y. Otani, Appl. Phys. Lett. **88**, 082501 (2006).
[7]C. W. J. Beenakker and H. van Houten, Phys. Rev. Lett. **63**, 1857 (1989).
[8]A. M. Gilbertson, M. Fearn, A. Kormányos, D. E. Read, C. J. Lambert, M. T. Emeny, T. Ashley, S. A. Solin, and L. F. Cohen, "Ballistic transport and boundary scattering in InSb/InAlSb mesoscopic devices," Phys. Rev. B (to be published).
[9]G.-D. Zhang, W.-G. Sun, S.-L. Xu, H.-Y. Zhao, H.-Y. Su, and H.-Z. Wang, J. Vac. Sci. Technol. A **27**, 681 (2009).
[10]R. J. Blaikie, D. R. S. Cumming, J. R. A. Cleaver, H. Ahmed, and K. Nakazato, J. Appl. Phys. **78**, 330 (1995).
[11]Y. Hirayama and S. Tarucha, Appl. Phys. Lett. **63**, 2366 (1993).
[12]O. J. Pooley, A. M. Gilbertson, P. D. Buckle, R. S. Hall, L. Buckle, M. T. Emeny, M. Fearn, L. F. Cohen, and T. Ashley, New J. Phys. **12**, 053022 (2010).
[13]N. Goel, S. J. Chung, M. B. Santos, K. Suzuki, S. Miyashita, and Y. Hirayama, Physica E (Amsterdam) **20**, 251 (2004).
[14]T. D. Boone, IEEE Electron Device Lett. **30**, 117 (2009).
[15]R. L. Kallaher, J. J. Heremans, N. Goel, S. J. Chung, and M. B. Santos, Phys. Rev. B **81**, 035335 (2010).
[16]C. H. Yang, M. J. Yang, K. A. Cheng, and J. C. Culbertson, Phys. Rev. B **66**, 115306 (2002).
[17]H. Akera and T. Ando, Phys. Rev. B **43**, 11676 (1991).